M. ROTH[1],✉
M. WEINELT[1]
T. FAUSTER[1]
P. WAHL[2]
M.A. SCHNEIDER[2]
L. DIEKHÖNER[2]
K. KERN[2]

Scattering of image-potential-state electrons by steps on Cu(001)

[1] Lehrstuhl für Festkörperphysik, Universität Erlangen-Nürnberg, Staudtstr. 7, 91058 Erlangen, Germany
[2] Max-Planck-Institut für Festkörperforschung, Heisenbergstr. 1, 70569 Stuttgart, Germany

ABSTRACT Scanning tunneling spectroscopy (STS) reveals a distinct asymmetry in the scattering properties of an isolated step for the $n = 1$ image-potential state on Cu(001). The elastic scattering probability for an electron traveling downstairs is determined from the strength of density oscillations in front of a step edge and is found to be approximately two times higher than for the opposite *upstairs* direction. A one-dimensional scattering model is extended to the case of asymmetric transmission and reflection coefficients. The calculations using the asymmetry measured by STS explain the dispersion and the decay rate of the $n = 1$ band on Cu(119) measured by two-photon photoemission. In particular, the asymmetry of the decay rate can be described quantitatively with a minimum of adjustable parameters. While the results can also be transferred successfully to the Cu(1115) surface, the limit of applicability is reached for Cu(117) with a step separation of 3.5 nearest-neighbor distances.

PACS 73.20.At; 79.60.Bm; 68.37.Ef; 72.10.Fk

1 Introduction

At metal surfaces the image-potential states arise in the attractive potential created by the interaction of an electron outside the surface with the polarization charge it induces [1]. Energy, dispersion, and lifetimes of these states have been studied for many low-index metal surfaces in detail by two-photon photoemission (2PPE) [2, 3] and excellent agreement with theoretical calculations is found [4]. With improving sensitivity and resolution of two-photon photoelectron spectroscopy the interest shifted to the influence of surface defects on the decay and dephasing of image-potential states [5, 6]. Steps on surfaces constitute a particularly simple class of defects which can easily be prepared with high density. The reduction of the symmetry compared to a low-index substrate leads to interesting effects in the dispersion and dynamics of image-potential states [3, 7–9].

Complementary to the momentum-resolved 2PPE are local measurements using scanning tunneling microscopy (STM) and spectroscopy (STS). STS measures the local density of states (LDOS) of the sample. It is used here to study the

✉ E-mail: m.roth@fkp.physik.uni-erlangen.de

scattering properties of a single step edge for image-state electrons on Cu(001). The interaction of surface-state electrons with defects at surfaces has been studied by STS before. The quantities extracted are the dispersion relation, lifetimes, reflectivities, and in some cases scattering phase shifts [10–16]. Similar measurements for image-potential states using STS were only recently reported [17].

In this paper we bring together the results from STS and 2PPE for the $n = 1$ image-potential state on Cu surfaces with terraces of (001) orientation. The reflectivity of an isolated step as determined by STS shows a pronounced asymmetric behavior depending on the direction of the electron motion parallel to the surface (upstairs/downstairs). Using a one-dimensional multiple-scattering model the measured asymmetry in the reflectivity can explain quantitatively the asymmetry in the decay rate observed in time-resolved 2PPE for Cu(119) and Cu(1115) [8].

2 Experimental results

For the STS studies a Cu(001) single-crystal sample was carefully prepared by sputtering and annealing cycles in UHV (base pressure 1×10^{-10} mbar). After cleaning, the sample was transferred in situ into a STM operating at 6 K. Spectroscopic measurements were performed using a lock-in technique with a modulation of the sample voltage of 10–30 mV RMS at a frequency of 4.5 kHz. All voltages are sample potentials measured with respect to the tip.

Figure 1a shows a topographic image of a step edge on Cu(001). A lower terrace on the left is separated from the upper terrace by a monatomic step. Along a horizontal line perpendicular to this step edge we performed $dI/dV(V, x)$ spectroscopy in the energy range where the $n = 1$ image-potential state is present. It is well known that the intense electric field in the tunneling junction will modify the image-potential states quite strongly (Stark effect) [18]. Therefore the onset of the $n = 1$ image-potential state is shifted by $+0.7$ eV and appears at a voltage of 4.7 V [17]. Mapping of $dI/dV(V, x)$ determines the LDOS at the bias voltage V as a function of the distance x from the step edge. An electron emitted from the STM tip will be elastically reflected at the step edge, leading to interference of the incoming wave with the reflected wave. As a result Friedel oscillations or 'standing waves' appear, analogous to the waves in the case of the
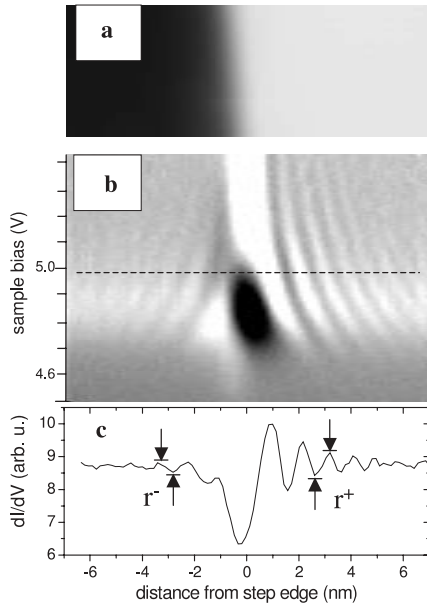
FIGURE 1 **a** STM topography (14 nm × 5 nm) of a step on Cu(001) taken at 5.2 V bias voltage. **b** $dI/dV(V, x)$ map taken along a horizontal line in **a** crossing the step edge. dI/dV is plotted in gray scale as a function of the lateral distance x from the step edge at $x = 0$ and of the bias voltage V. At bias voltages where the $n = 1$ image state overlaps with the Fermi level of the tip, electrons injected into the state are partially reflected elastically at the step edge and return coherently to the tip. Thereby an interference pattern is created. **c** $dI/dV(x)$ for $V = 4.95$ V (*dashed line* in **b**). The amplitude of the dI/dV signal is proportional to the reflection coefficients $r^{\pm}$ of the respective sides of the step. From the amplitudes taken at the positions of the arrows we obtain a ratio $r^{+}/r^{-} \approx 2.4$

surface states of the noble metal (111) surfaces (Fig. 1b). We note, however, that there are deviations from that analogy for distances $x < 1$ nm from the step edge and bias voltages below 5.0 V. This might be indicative of a step-induced state as was observed recently for steps on Cu (111) [19]. From the wavelength of the interference pattern as a function of energy one can determine the dispersion relation and from the spatial decay of the pattern the phase-coherence time of electrons in that state [13, 17]. Both agree quantitatively with the results from time-resolved 2PPE [2, 20] showing that the motion of the electrons parallel to the surface is not affected by the presence of the STM tip [17]. This result can be understood from the observation that although the $n = 1$ state shifts by as much as 0.7 eV in the field of the tip it is still located approximately at the center of the ~ 6 eV-wide directional band gap of Cu(100). Thus, the coupling to the bulk electrons does not change appreciably, which determines the dynamics of the image-potential-state electrons [20]. The amplitude of LDOS modulation is proportional to the probability r for an electron to be reflected elastically at the step edge. If we now compare amplitudes of the standing waves on the upper and the lower terraces one sees immediately that the electrons coming from the lower terrace (traveling 'upstairs' in the case of vicinal Cu(001) surfaces) experience a much lower elastic backscattering rate compared to the electrons on the upper terrace. Such a behavior was also observed in the case of the surface-state electrons. However in the case of image-potential states it is much more pronounced. A quantitative comparison of the amplitudes of the electron waves on the upper terrace (r^{+}

in Fig. 1c) to those of the electrons on the lower terrace (r^{-}) taken in the far field of the step-induced density modulations reveals that $r^{+}/r^{-} \approx 2.4$. (This ratio is 1.5 or smaller in the case of the surface-state electrons scattering at a step edge on Ag(111) [12].)

Experimental details and results for time- and momentum-resolved 2PPE on a Cu(119) surface have been reported before [7–9, 21]. The energy dispersion and the decay rate of the $n = 1$ image-potential state are plotted as a function of parallel momentum $k_{\parallel}$ in a reduced zone scheme in Fig. 2. The measured energy bands are close to the free-electron parabola (dashed lines) with a somewhat worse agreement for data obtained outside the first Brillouin zone (open symbols). The decay rate shows a pronounced asymmetry with larger values for electrons traveling downstairs ($k_{\parallel} < 0$) compared to the upstairs direction ($k_{\parallel} > 0$) [8, 9, 21]. This observation has been attributed to intraband scattering with a preference towards the upstairs direction [21] on the basis of similar unidirectional interband-scattering processes between image-potential bands [8, 21]. A constant decay rate of 43 meV was subtracted from the experimental data. The plotted values represent therefore the variation of the decay rate with the lateral motion.

Additional data have been obtained on a Cu(1115) sample. The results are qualitatively similar to the ones for the Cu(119) surface. The energy dispersion of the $n = 1$ image-potential state on Cu(1115) follows the free-electron behavior within the first Brillouin zone and the corresponding data points are not shown in Fig. 2. The points for the decay rate are plotted as circles, and the open circles were obtained outside the first surface Brillouin zone and shifted by the addition of a suitable
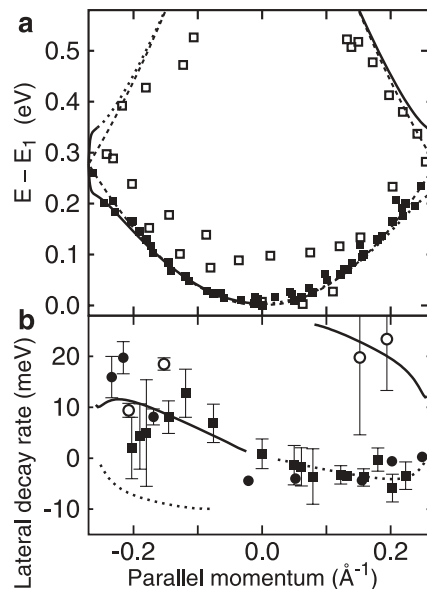

FIGURE 2 **a** Energy dispersion for the $n = 1$ image-potential state on Cu(119) as a function of parallel momentum. Data points measured outside the first surface Brillouin zone are marked by *open symbols*. **b** Decay rate after subtraction of an average constant. Results for Cu(1115) are shown as *circles* and have been scaled with the ratio of the lattice vectors for direct comparison with the Cu(119) data (*squares*). Experimental data points were obtained by time-resolved two-photon photoemission. *Curves* are calculated with a one-dimensional scattering model for the motion parallel to the surface

reciprocal-lattice vector. After subtraction of a constant decay rate of 29 meV the data have been scaled on both axes with the factor $a(1115)/a(119)$ for direct comparison of the lateral decay rate with the model of Sect. 3. With this scaling the data sets between the two surfaces agree remarkably well.

3   One-dimensional scattering model

The scattering properties for a single step can be used to evaluate the properties of a regular array of scatterers as long as the separation between steps is sufficiently large. As sketched in Fig. 3 the model potential for a vicinal surface is composed of individual barriers separated by a distance a in the direction parallel to the surface and perpendicular to the step edges. The constant potential in a (possibly infinitely small) region between the steps is conveniently chosen to be zero. Motivated by the STS results we extend the one-dimensional multiple-scattering formalism [22–24] to the case of an asymmetry of the transmission (t) and reflection (r) coefficients for waves coming from the right ($+$) and left ($-$), respectively. The model is used in Sect. 4 to explain the observed asymmetry in the decay rate for image-state electrons traveling in different directions on vicinal Cu(001) surfaces.

In the region of constant potential ($x = -a/2$) the wave function can be expanded into plane waves

$$\psi(x) = Ae^{iKx} + Ar^-e^{-iKx} + Bt^+e^{-iKx} . \tag{1}$$

From Fig. 3 the interpretations of the various terms are a wave of amplitude A traveling to the right that is reflected by the potential barrier towards the left with a reflection coefficient r^- and a wave of amplitude B which has been transmitted through the barrier at the right with a transmission coefficient t^+. At $x = a/2$ the wave function can be written

$$\psi(x) = Be^{-iKx} + Br^+e^{iKx} + At^-e^{iKx} . \tag{2}$$

The wave vector K is given by the energy $E = \hbar^2 K^2/2m$, where m denotes the (effective) mass of the electron. From Fig. 3, the ansatz (1) and (2) only the wave vectors with $\mathrm{Re}(K) > 0$ are consistent with the model. Absorption or damping of the wave functions may be included by an imaginary part V_i of the inner potential [23, 25].

The solutions in the periodic potential with period a must obey Bloch's theorem with wave vector $k = k_{||}$:

$$\psi(x+a) = e^{ika}\psi(x) \tag{3}$$

for all x. With Bloch's theorem we can evaluate the wave function of (1) at $x = a/2$, which has to be equal to (2). The same procedure has to be applied to the derivatives of the wave functions. With the abbreviation $\alpha = \exp(iKa)$ the following quadratic equation for $\beta = \exp(ika)$ is obtained:

$$t^+\beta - ((t^+t^- - r^+r^-)\alpha + 1/\alpha) + t^-/\beta = 0 . \tag{4}$$

The two solutions β_1 and β_2 are related by $\beta_1\beta_2 = t^-/t^+$ and give, in general, complex solutions for the Bloch wave vector k. The two solutions are related by

$$k_1a = -k_2a + i\ln(t^+/t^-) . \tag{5}$$

For the common case of $t^+ = t^-$ we obtain the complete symmetry for the right- and left-traveling Bloch waves with the solutions $k_1 = -k_2$. For real, but different, transmission coefficients there is a constant shift of the imaginary part of the wave vector and the real parts retain the symmetry $\mathrm{Re}(k_1) = -\mathrm{Re}(k_2)$. It is interesting to note that the asymmetry in the wave vectors is caused only by the transmission coefficients that determine the decay of the wave function from unit cell to unit cell. The amplitudes of the wave functions also contain the reflected waves, as can be seen by the following relationship between the amplitude ratios A/B:

$$(A/B)_1(A/B)_2 = r^+t^+/r^-t^- . \tag{6}$$

Solutions of (4) are plotted in Fig. 4 together with free-electron bands (dashed lines) for comparison. The parameters were chosen to be $t^+ = \sqrt{0.2}$, $r^+ = i\sqrt{0.8}$, $t^- = \sqrt{0.8}$, and $r^- = i\sqrt{0.2}$. The purely imaginary reflection coefficients describe a phase shift by π upon reflection [23]. The parameter set fulfills the condition $|t^\pm|^2 + |r^\pm|^2 = 1$, although the formalism includes the case with absorption $|t^\pm|^2 + |r^\pm|^2 < 1$. The imaginary part of the wave vector is finite for all energies (even for $V_i = 0$) and different for the two solutions, because $t^+ \neq t^-$. The transmission coefficient t^- (t^+) influences mainly the damping of the branches with positive group velocity $v = \hbar^{-1}dE/d\,\mathrm{Re}(k) > 0$ ($v < 0$) as suggested by the ansatz in Fig. 3.

All solutions plotted in Fig. 4 have a significant imaginary part of the wave vector. This implies that the wave function
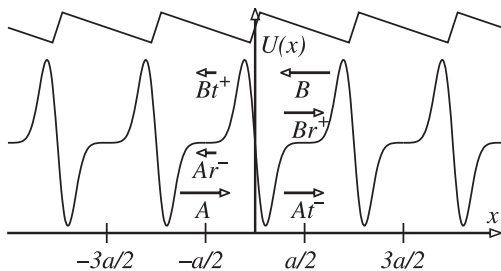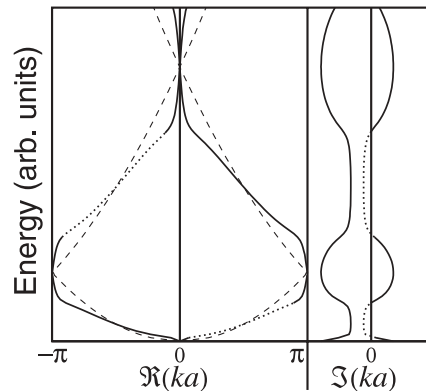

FIGURE 3 Schematic of a stepped surface and the corresponding potential. The wave function between the steps is described by a superposition of waves of amplitudes A and B traveling to the *right* and *left*, respectively. The fractions $t^\pm$ are transmitted and $r^\pm$ are reflected

FIGURE 4 Complex band structure from (4). *Solid* and *dotted lines* correspond to the exponentially decaying and increasing solutions, respectively. The free-electron bands are plotted for comparison (*dashed curves*)

grows exponentially in either the $+x$ or $-x$ direction. Meaningful solutions have to decay exponentially in the direction given by the group velocity v. The dotted lines in Fig. 4 show branches with exponentially increasing solutions in the traveling direction of the electron wave. The introduction of a small imaginary potential into the energy removes this unphysical situation. The exponentially decaying solutions do not imply a loss of total current, but have to be interpreted as the scattering into other channels, e.g. bulk bands [25], which are not explicitly included in the one-dimensional model. For a strict one-dimensional problem $r^+ = r^-$, $t^+ = t^-$, and $|t|^2 + |r|^2 = 1$ is required [22].

4   Discussion

Figure 2 shows the results of a calculation with the one-dimensional scattering model using $r^+ = i\sqrt{0.27}$. From the STS results we then obtain $r^- = r^+/2.4 = i\sqrt{0.05}$. The coefficients $t^+ = \sqrt{0.73}$ and $t^- = \sqrt{0.95}$ were chosen under the condition $|t^\pm|^2 + |r^\pm|^2 = 1$. The damping of the wave function given by the imaginary part of the wave vector $\text{Im}(k)$ in the x direction is converted to a decay rate in time by multiplication with the group velocity $v(k)$. The result is shown as a lateral energy-decay rate (after multiplication with $\hbar$) by the curves in Fig. 2b. Near the zone boundaries and at the bottom of the band the decay rate diverges. The corresponding sections have been omitted in the plots of Fig. 2b. The dotted parts of the curves represent exponentially increasing solutions (see also Fig. 4). The lateral decay rate decreases linearly with parallel momentum, because $\text{Im}(k)$ is negative and approximately constant outside the band gaps (see Fig. 4) and the group velocity (in the free-electron case) is proportional to k. The additional branches correspond to higher energies and are shifted into the first Brillouin zone in the reduced zone scheme.

Energy and momentum have been scaled in Fig. 2a for the case of a Cu(119) surface. The corresponding 2PPE data for the $n = 1$ image-potential state on Cu(119) are shown by squares. Data points measured outside the first surface Brillouin zone have been shifted by the addition of the appropriate reciprocal-lattice vector into the first zone and are marked by open symbols. The measured as well as the calculated dispersion is close to the free-electron bands shown by dashed lines. The calculated energy gap of $\approx 100\,\text{meV}$ is in reasonable agreement with previous estimates of $\approx 80\,\text{meV}$ with a scattering model without damping [7, 9]. The transmission coefficient of 0.96 ± 0.02 determined in the cited work corresponds nicely to the value of $t^- = \sqrt{0.95}$ in the present model. A direct comparison is hindered by the intrinsic damping from the asymmetry of the transmission coefficients. This leads to a smearing of the band edges similar to the case with an imaginary part of the potential [23].

The decay rates measured on the Cu(119) surface are shown in Fig. 2b by solid squares. A constant decay rate of $43\,\text{meV}$ was subtracted from the experimental values. This reflects the decay into the bulk states via electron–electron scattering, which is not included in the present model. Data and calculations shown in Fig. 2b represent the change of the decay with parallel momentum. This is consistent with the one-dimensional scattering model, which describes only the motion of the electrons parallel to the surface. Modeling the decay into bulk states by the introduction of an imaginary potential V_i is possible. The resulting decay rates show a similar dependence on k; however, the divergence of the decay rate spans larger k regions.

The agreement between experiment and calculation is surprisingly good considering that the differences in the decay rates are only about 10 meV, corresponding to a lifetime variation of 4 fs [21]. For the comparison to the model only the reflection coefficient r^+ was adjusted in accordance with the experimental dispersion. The results of the STS experiments then determine the coefficient r^-. For simplicity no further parameters like absorption, imaginary part of the potential, or phase shifts have been included. In particular, the absorption ($|t^\pm|^2 + |r^\pm|^2 < 1$) is conceptually needed to explain the asymmetric reflection coefficients. Calculations including absorption give similar results as shown in Fig. 2. The 2PPE data do not permit a unique selection of additional parameters.

The transfer of the scattering properties of a single step to a periodic step lattice should apply also to surfaces with other step densities. The circles in Fig. 2b show results for Cu(1115). The data have been scaled on both axes[1] with the ratio of the lattice vectors for direct comparison with the calculations adjusted to the Cu(119) periodicity. A constant of 29 meV has been subtracted from the experimental values representing the average decay rate into bulk states. The agreement with the calculated curves is good in particular also for the data points from the second Brillouin zone (open circles) at positive $k_{||}$.

For Cu(117) an upper limit for the lifetime difference between upstairs and downstairs directions of 2 fs has been found [21]. According to our model the asymmetry should be even larger than for Cu(119). One explanation for this discrepancy could be that, at a step separation of 3.5 nearest-neighbor distances, the scattering properties of the step lattice differ from those of an isolated step. The dipole–dipole interaction would lead to a weakening of the effective potential strength. From the STS data in Fig. 1 we see that for distances very close to the step edge ($x \leq 1\,\text{nm}$) the interference pattern deviates from the behavior expected for hard-wall scattering at the step edge. For Cu(117) the surface-projected bulk band structure indicates a significant narrowing of the band gap even when umklapp processes are neglected [7, 9]. The resulting increase of the phase space for scattering into bulk bands might take over the importance of the scattering by the steps parallel to the surface.

The Cu(119) surface exhibits a much broader distribution of terrace widths compared to the Cu(117) surface, and actually has an orientation closer to Cu(118) with an equal probability of (117) and (119) terraces [21]. The major conclusions of the present work are not affected by the different surface orientation. It would be interesting to extend the one-dimensional scattering model to the case of the disordered step arrangement obtained from the STM measurements of [21].

---

[1] The axes correspond to the real and imaginary parts of the wave vector, which scales with the lattice periodicity. The imaginary part is multiplied by the group velocity, which is independent of the k scale.

5   Conclusions

In this paper we discussed the scattering properties of surface steps as experienced by image-potential-state electrons. We bring together results from non-local, but momentum- and time-resolved, 2PPE and local measurements using STS. STS reveals a distinct asymmetry in the reflectivity of an isolated step for the $n = 1$ image-potential state on Cu(001). This finding is used in a one-dimensional scattering model to explain the dispersion and the decay rate of the $n = 1$ band on Cu(119) measured by 2PPE. In particular, the asymmetry of the decay rate can be described quantitatively with a minimum of parameters determined by experimental data. While the results can also be transferred successfully to a Cu(1115) surface, the limit of applicability is reached for a Cu(117) surface with a step separation of only 3.5 nearest-neighbor distances.

REFERENCES

1 P.M. Echenique, J.B. Pendry: J. Phys. C: Solid State Phys. **11**, 2065 (1978)

2 T. Fauster, W. Steinmann: In *Photonic Probes of Surfaces*, Vol. 2 of *Electromagnetic Waves: Recent Developments in Research*, ed. by P. Halevi (North-Holland, Amsterdam 1995) Chapt. 8, p. 347

3 R.M. Osgood, X.Y. Wang: In *Solid State Physics*, Vol. 51, ed. by H. Ehrenreich, F. Spaepen (Academic, San Diego 1997)p. 1

4 P.M. Echenique, J.M. Pitarke, E.V. Chulkov, V.M. Silkin: J. Electron Spectrosc. Relat. Phenom. **126**, 163 (2002)

5 T. Fauster, Ch. Reuß, I.L. Shumay, M. Weinelt: Chem. Phys. **251**, 111 (2000)

6 K. Boger, M. Weinelt, T. Fauster: Appl. Phys. A, DOI: 10.1007/s00339-003-2312-4

7 M. Roth, M. Pickel, J. Wang, M. Weinelt, T. Fauster: Appl. Phys. B **74**, 661 (2002)

8 M. Roth, M. Pickel, J. Wang, M. Weinelt, T. Fauster: Phys. Rev. Lett. **88**, 096 802 (2002)

9 M. Weinelt: J. Phys.: Condens. Matter **14**, R1099 (2002)

10 M.F. Crommie, C.P. Lutz, D.M. Eigler: Science **262**, 218 (1993)

11 J. Li, W.-D. Schneider, R. Berndt, O.R. Bryant, S. Crampin: Phys. Rev. Lett. **81**, 4464 (1998)

12 L. Bürgi, O. Jeandupeux, A. Hirstein, H. Brune, K. Kern: Phys. Rev. Lett. **81**, 5370 (1998)

13 L. Bürgi, O. Jeandupeux, H. Brune, K. Kern: Phys. Rev. Lett. **82**, 4516 (1999)

14 J. Kliewer, R. Berndt, E.V. Chulkov, V.M. Silkin, P.M. Echenique, S. Crampin: Science **288**, 1399 (2000)

15 L. Vitali, P. Wahl, M.A. Schneider, K. Kern, V.M. Silkin, E.V. Chulkov, P.M. Echenique: Surf. Sci. **523**, L47 (2003)

16 M.A. Schneider, L. Vitali, N. Knorr, K. Kern: Phys. Rev. B **65**, 121 406 (2002)

17 P. Wahl, M.A. Schneider, L. Diekhöner, R. Vogelgesang, K. Kern: Phys. Rev. Lett. **91**, 106 802 (2003)

18 G. Binnig, K.H. Frank, H. Fuchs, N. Garcia, B. Reihl, H. Rohrer, F. Salvan, A.R. Williams: Phys. Rev. Lett. **55**, 991 (1985)

19 L. Bartels, S.W. Hla, A. Kühnle, G. Meyert, K.-H. Rieder, J.R. Manson: Phys. Rev. B **67**, 205416 (2003)

20 W. Berthold, U. Höfer, P. Feulner, E.V. Chulkov, V.M. Silkin, P.M. Echenique: Phys. Rev. Lett. **88**, 056805 (2002)

21 M. Roth, M. Pickel, M. Weinelt, T. Fauster: Appl. Phys. A, DOI: 10.1007/s00339-003-2311-5

22 N.W. Ashcroft, N.D. Mermin: *Solid State Physics* (Saunders College, Philadelphia 1976) Chapt. 8, Problem 1

23 J.B. Pendry: *Low Energy Electron Diffraction* (Academic, London 1974) Chapt. IIIB

24 T. Fauster: Appl. Phys. A **59**, 639 (1994)

25 G. Hörmandinger, J.B. Pendry: Phys. Rev. B **50**, 18 607 (1994)